
This is an electronic reprint of the original article.
This reprint may differ from the original in pagination and typographic detail.

Patikiri Arachchige, Diluka; Zhou, Quan

Learning to Shape Liquid Droplets on an Air-Ferrofluid Interface with Sequences of Actuation

Published in:

2023 International Conference on Manipulation, Automation and Robotics at Small Scales (MARSS)

DOI:

[10.1109/MARSS58567.2023.10294154](https://doi.org/10.1109/MARSS58567.2023.10294154)

Published: 13/10/2023

Document Version

Peer reviewed version

Please cite the original version:

Patikiri Arachchige, D., & Zhou, Q. (2023). Learning to Shape Liquid Droplets on an Air-Ferrofluid Interface with Sequences of Actuation. In S. Haliyo, M. Boudaoud, M. A. Qasaimah, & S. Fatikow (Eds.), *2023 International Conference on Manipulation, Automation and Robotics at Small Scales (MARSS)* (pp. 1-6). Article 10294154 IEEE. <https://doi.org/10.1109/MARSS58567.2023.10294154>

This material is protected by copyright and other intellectual property rights, and duplication or sale of all or part of any of the repository collections is not permitted, except that material may be duplicated by you for your research use or educational purposes in electronic or print form. You must obtain permission for any other use. Electronic or print copies may not be offered, whether for sale or otherwise to anyone who is not an authorised user.

Learning to Shape Liquid Droplets on an Air-Ferrofluid Interface with Sequences of Actuation

P. A. Diluka Harischandra and Quan Zhou

Abstract—Shape morphing of liquid droplets is important for advances in both medical and industrial applications. However current manipulation techniques lack methods to control shapes other than elliptical-shaped droplets. Here we propose using Long Short-Term Memory (LSTM) based model to learn and predict the evolution of the shape of a non-magnetic liquid droplet at an air-ferrofluid interface deformed with programmed sequential actuation of electromagnets. The resulting droplet shapes can be convex or concave. We can also predict the actuation sequences for a given shape sequence with an accuracy of 79.1 %. The proposed method could also be applied to a variety of other liquid droplet shape-morphing systems which utilize arrays of electromagnetic or electric actuators.

Index Terms - liquid shaping, electromagnet, programmable morphologies, air-liquid interface, long short-term memory (LSTM)

I. INTRODUCTION

Shape morphing of liquids into non-equilibrium shapes is a fundamental research topic that may impact many applications in industry [1]–[5] such as printing and coating [4], optical engineering [5] and, biological sciences including tissue engineering [6]–[8]. The advancement of these applications depends on the capability to control the shape of the liquid, yet this capability is still in its infancy.

Recently, numerous techniques have been proposed to manipulate liquids using an external energy field. A spherical-shaped liquid droplet can be transformed into an elongated shape or other shapes using airflow [9], acoustic [10], electric [11]–[13], thermal [14], and magnetic fields [15]–[18]. Liquid droplets can be levitated by airflow [9] or acoustic fields [10], resulting in star-shaped oscillations in the droplets. There is also abundant literature on deforming liquid droplets using electric fields [19]. External electric fields can induce the formation of spontaneous patterns in specific oil mixtures, leading to the emergence of non-equilibrium fluidic lattices and droplets that take the form of polygonal or toroidal shapes [11]. Electric fields can also be used for programmable shape manipulation of liquid metals [12]. The shape of oil droplets in an emulsion of oil and water can vary depending on the types of surfactants used and the rate at which they are cooled. They can take the form of hexagonal or triangular platelets or elongated asperities [14]. Similarly, liquid crystal droplets in a water-based solution can transform into elongated filaments under specific cooling conditions [20]. Photothermally induced pyroelectric effects can be used to elongate a water droplet situated on a superhydrophobic surface [13]. There is also

noticeable progress in shaping magnetic liquids such as ferrofluids. Ring magnets can be used to form ring-shaped or C-shaped ferrofluid droplets, which can then be employed to transport hydrogel balls [15]. Magnetic fields can also be utilized to move or stretch liquid metal droplets mixed with iron nanoparticles into a cross-shaped pattern [18].

Some works utilize an array of actuators to deform the droplets into several shapes, depending on the active actuators [12], [15], [18]. However, these works have not explored the possibility of learning the evolution of shape due to sequential actuation. Although a ferrofluid droplet can be directly manipulated using magnetic fields to deform the droplet into an elliptical shape and control the stretch length orientation position by using an electromagnetic coil system [16], current methods lack the capability to understand more complex shapes. Consequently, the control of the shape of liquid droplets is limited to elliptical shapes as demonstrated in previous research.

In our recent work, we have made significant advancements toward the manipulation of the shape of liquid droplets at an air-ferrofluid interface into a variety of morphologies other than elliptical shapes using magnetic fields [21]. The findings of our previous work highlight the need for a methodology to understand and learn more complex shapes in droplets. Furthermore, we have also demonstrated how sequential actuation can shape the droplet at an air-ferrofluid interface.

In sequential actuation, the current state of the droplet is influenced by several factors such as the inertia of the droplet, the initial shape and area of the droplet, and the magnetic remanence resulting from previous actuation. Hence, it is crucial to establish a mechanism to capture and retain the sequence of droplet morphology changes.

In this paper, we propose using an LSTM (Long Short-Term Memory) based model to predict the deformation of a non-magnetic liquid droplet at the air-ferrofluid interface due to the sequential magnetic fields applied by eight electromagnetic actuators. LSTM models capture temporal dependencies; therefore, they can model complex relationships between past actuation and their impact on future actuation. LSTM-based models are widely used for natural language processing tasks and robot applications because of the distinct structure of the gating mechanisms and memory cells of LSTMs which allows them to capture complicated relationships rapidly and effectively overcome the disadvantages of traditional Recurrent Neural Networks (RNN) such as the vanishing gradient problem [22], [23].

*This work was supported by Academy of Finland (grant #317018).

P. A. Diluka Harischandra and Quan Zhou are affiliated with the Department of Electrical Engineering and Automation, School of Electrical

Engineering, Aalto University, 02150 Espoo, Finland (e-mail: diluka.harischandra@aalto.fi, quan.zhou@aalto.fi).

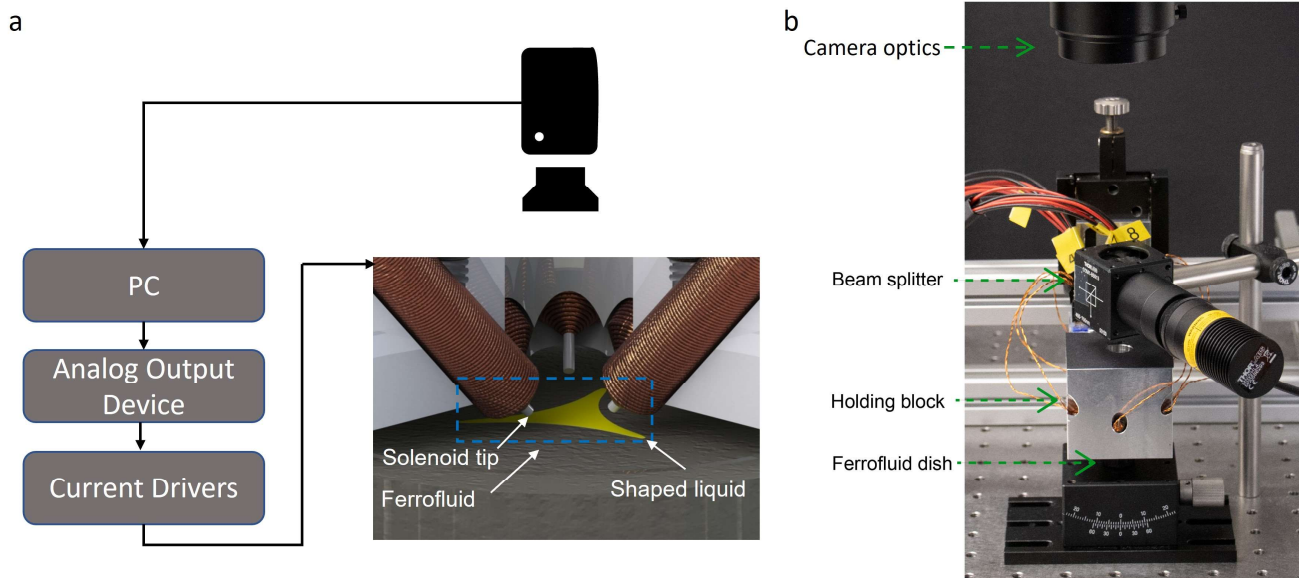


Figure 1. a) Schematic of the experimental setup and a CAD illustration of the arrangement of the solenoids and the shaped liquid at the air-ferrofluid interface. b) Experimental setup

LSTMs have also been applied in learning the forward kinematics of surgical robotics, where the collection of large amounts of data is expensive or risky [24]. In this work, we also study the ability to predict the required actuation sequence for a target shape by learning the inverse problem with an LSTM model.

II. METHODS

A. Experimental Setup

The experimental setup is adapted from our previous work for the manipulation of liquids at the air-ferrofluid interface [21] and is shown in Fig 1. It consists of eight electromagnetic solenoids, each with 300-400 turns of SWG 27 copper wire in six layers wrapped around a 1 mm diameter martensitic steel wire. The solenoids are driven using eight current controllers (ESCON 50/5, Maxon Group, Switzerland). The current controllers are supplied with a constant voltage of 12 V through a low-noise power source (E36233A, Keysight, USA). We actuate the solenoids with ramped signals generated by an analog output device (PCIe-6738, National Instruments) to minimize the vibration of the surface of the fluid. The solenoids were calibrated by using a Hall effect sensor (SS495A1, Honeywell, USA) to measure the magnetic flux density at the tip of the solenoid.

We used 25 mT magnetic flux density at the tip for the sequential actuation. To improve the repeatability of the sequences we first center the droplet actuating all solenoids with 30 mT magnetic flux density. Then to minimize the effects of magnetic remanence all solenoids are demagnetized before the actuation of the sequence, using an exponentially decaying sinusoidal current signal given by $I = Ae^{-kt}\text{Sin}(\omega t)$, where amplitude $A = 2$ A, rate of decay $k = 2.5$, and the sine frequency $\omega = 50$ rad s^{-1} . A sequential actuation experiment is shown in Fig. 2a consisting of the initial state (i), first actuation (ii), and the second actuation (iii). Actuated solenoids are marked with green indicators and deactivated solenoids are

marked with red indicators. Cardinal and intercardinal directions are used to denote the solenoids. During the sequence, the solenoids are actuated in a ramp to 25 mT in one second and held at that level for 1.5 seconds, and then switched to the next actuation in a ramp in one second and held at that level for 3.5 seconds.

We use a commercial ferrofluid (EMG 408, Ferrotec, USA) diluted with Milli-Q Ultrapure water by volume at a 1:7 ratio. The dish is initially overfilled with the ferrofluid and then the air-ferrofluid interface is flattened by removing the excess fluid. We use ~ 0.2 μL of n-hexadecane as the manipulated liquid. Table I show the properties of the manipulated liquids. The hexadecane droplet spreads at the air-liquid interface due to its positive spreading coefficient [21], resulting in an increase in surface area during the experiments. The spread area, in addition to actuated solenoids, significantly impacts the final droplet shape.

Image acquisition is performed by a color camera (Point Gray GS3-U3-41C6C-C, FLIR Systems Inc., Canada). The workspace is illuminated using a 50:50 beam splitter (CCM1-BS013, Thorlabs Inc.), a collimation lens, and a LED source (MNWHL4, Thorlabs Inc.). Image and data recording is performed at 10 Hz frequency using an in-house developed C++-based software.

B. Data preprocessing

Although deep learning models can potentially learn directly from raw camera data, they necessitate a substantial amount of data to achieve accurate results. We circumvent this problem by preprocessing the input image and providing a

TABLE I. PROPERTIES OF MANIPULATION LIQUIDS

Liquid	Surface Tension (mN m^{-1})	Density (gcm $^{-3}$)	Viscosity (mPa·s)
Ferrofluid	70.88	0.99123	3.558
Hexadecane	27.39	0.76851	1.138

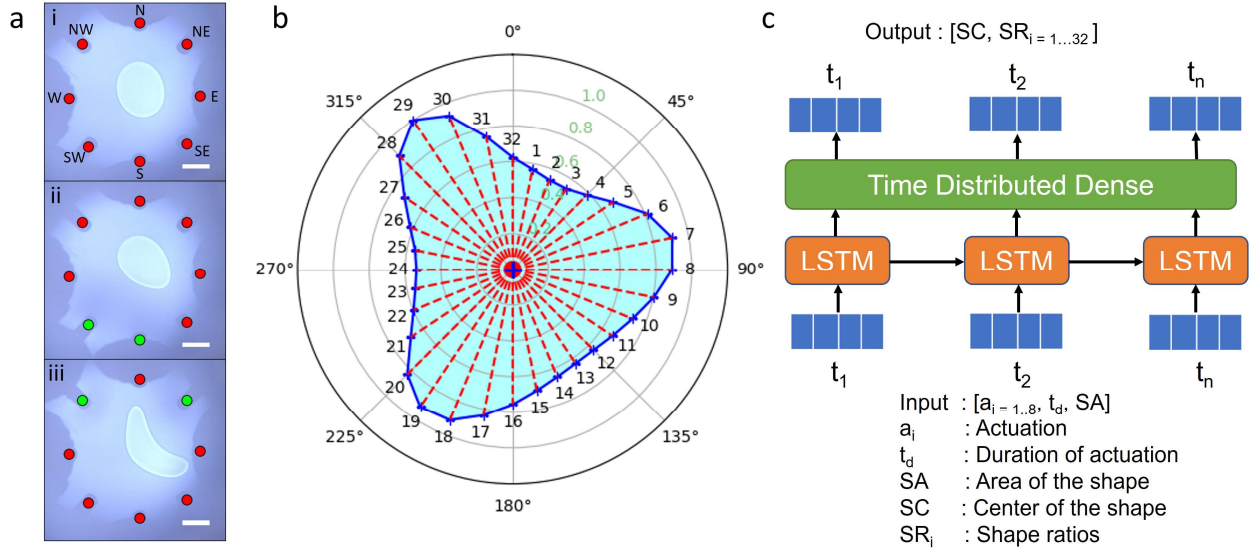


Figure 2. a) Experimental data of a hexadecane droplet at the air-ferrofluid interface for the initial state and two sequential actuations of the solenoids b) Shape representation with 32 segments along the contour of the shape c) LSTM-based model for shape prediction. The scale bars are 2 mm.

shape representation as input to the LSTM model. Several sequential steps are carried out in our image processing pipeline. The input image is first cropped and converted to grayscale. Following that, adaptive thresholding is performed, and the resulting image is inverted using a bitwise not operation. To eliminate unwanted artifacts, a closing morphological operation is performed. Finally, contour detection is performed on the image to obtain the droplet boundary.

This contour of the droplet shape is divided into 32 segments based on angle as shown in Fig. 2b. The number of segments was determined empirically based on the shapes observed in the experimental data. A higher number of segments will reduce aliasing errors of the predicted shape but also increase the complexity of the model. The Euclidean distance from the center of the shape to each intersection point can then be calculated. These distances are then divided by the maximum distance to obtain a size-invariant measure of the shape.

The area of the shape is an important parameter in the shape representation due to the spreading phenomena of the hexadecane droplet at the air-ferrofluid interface. The area of the contour is obtained using the OpenCV function `contourArea`, which is based on Green's theorem. Therefore, the shape is represented by the relative distances from the center coordinates of the shape to the intersection points $SR_{i=1...32}$, as well as the center of the shape SC, and its area SA.

C. Shape prediction

To predict the shape given a sequence of actuation we can train a sequence-to-sequence (Seq2Seq) LSTM model as shown in Fig. 2c. The input to the model consists of the actuation state of the eight solenoids $a_{i=1...8}$, time duration of the actuation t_d , and the area SA of the shape contour. The output of the model is the shape representation which consists

of the center of the shape SC and the relative distances to the intersection points $SR_{i=1...32}$.

The model consists of an LSTM layer with a 300-dimensionality output followed by a time distributed dense layer of 34 neurons with sigmoid activation. The output of this layer corresponds to the shape representation $SR_{i=1...32}$ and the center coordinates of the shape SC. Fig. 3 shows the schematic representation of an LSTM cell [22]. An LSTM cell consists of three gates: the input gate, the forget gate, and the output gate, each governed by equations (1), (2), and (3) which allow the LSTM to selectively control the flow of information. x_t and h_t denote the input and hidden state. The weight matrices W_*, U_* and bias vectors b_* are learned during the training phase. Each of the gates has the same inputs x_t and h_{t-1} but the parameters W_*, U_*, b_* are decoupled, allowing the gates to operate independently. The sigmoid function σ modulates the inputs to the gates to values in the range of 0-1. The input gate i_t determines which new information x_t and the previous hidden state h_{t-1} should be incorporated into the cell state. The forget gate f_t determines how much information to forget from the previous cell state.

$$i_t = \sigma(W_i x_t + U_i h_{t-1} + b_i) \quad (1)$$

$$f_t = \sigma(W_f x_t + U_f h_{t-1} + b_f) \quad (2)$$

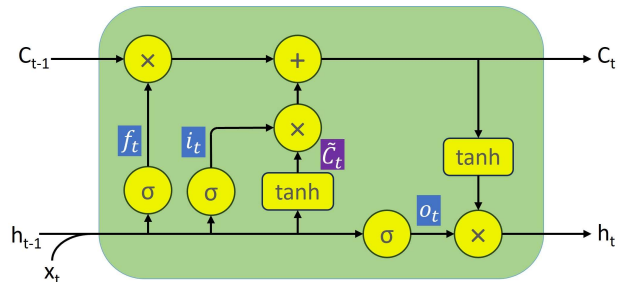


Figure 3. Schematic diagram of an LSTM network

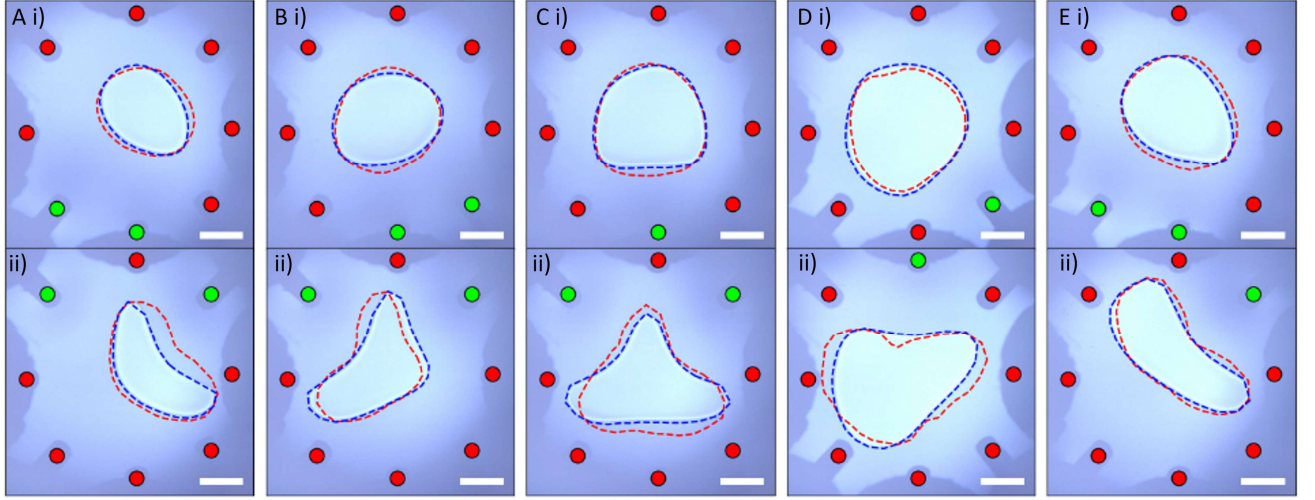


Figure 4. Validation results for shape prediction of a hexadecane droplet at the air-ferrofluid interface for five sequences. The blue and red dashed lines show the actual and predicted contours, respectively. Actuated solenoids are marked with green indicators and deactivated solenoids are marked with red indicators. The scale bars are 2 mm.

$$o_t = \sigma(W_o x_t + U_o h_{t-1} + b_o) \quad (3)$$

The candidate cell state \tilde{C}_t is computed with inputs x_t and h_{t-1} and has the hyperbolic tangent activation as shown in (4). The operator \odot denotes element-wise product. The cell state C_t is updated based on previous cell state C_{t-1} and candidate cell state \tilde{C}_t depending on the input and forget gates as shown in (5). Lastly, the hidden state h_t is updated based on the output gate o_t and the current cell state C_t with hyperbolic tangent activation as shown in (6).

$$\tilde{C}_t = \tanh(W_c x_t + U_c h_{t-1} + b_c) \quad (4)$$

$$C_t = f_t \odot C_{t-1} + i_t \odot \tilde{C}_t \quad (5)$$

$$h_t = o_t \odot \tanh(C_t) \quad (6)$$

The model is implemented using Keras and TensorFlow python libraries and trained with an NVIDIA RTX 2080 Ti GPU. The length of the sequence is not fixed so the network can be adapted to sequences with different lengths. The model is trained for 500 epochs using mean absolute error loss.

D. Inverse model

We used the same dataset for training an inverse model to predict the required actuation sequences given a target shape sequence. The model closely resembles the shape prediction model, with a few changes in the input, output size, and number of LSTM cells. The input for the inverse model includes the relative distances from the center of the shape to the intersection points $SR_{i=1..32}$, as well as the center of the shape itself SC , its area SA , and the duration of the actuation t_a . The model consists of an LSTM layer with a 100-dimensionality output which is fed to a time distributed dense layer of eight neurons with sigmoid activation. The sigmoid outputs are transformed to a binary representation which corresponds to the actuation $a_{i=1..8}$ by applying a threshold of 0.5 on the sigmoid output. The model is trained using the binary cross entropy loss for 500 epochs.

III. RESULTS

We have collected 116 experimental data samples focusing on sequences of only two actuations since the number of actuation combinations grows exponentially with the number of steps in the sequences. Each data sequence in our collected dataset includes the initial state of the system, followed by the states observed after each actuation. The dataset primarily consists of actuation combinations of three solenoids on the top side (NE, N, NW) and the three solenoids on the bottom side (SE, S, SW). The opposite motions caused by the actuations cancel out and keep the droplet near the center of the workspace. The dataset was split with a 20% test-train ratio.

The validation test results for shape prediction of five sequences of two actuation are shown in Fig. 4. For comparing the predicted and actual shape, the predicted shape is plotted relative to the actual center of the shape. The error between the predicted and actual center of the area for the first and second actuation of the samples of the validation dataset are 0.40 ± 0.18 mm and 0.40 ± 0.27 mm, respectively.

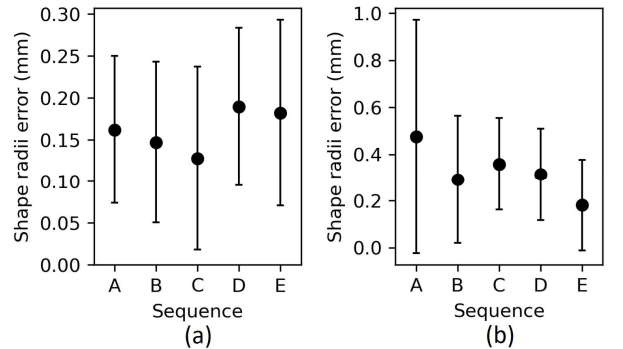


Figure 5. Shape prediction error (a) First actuation (b) Second actuation

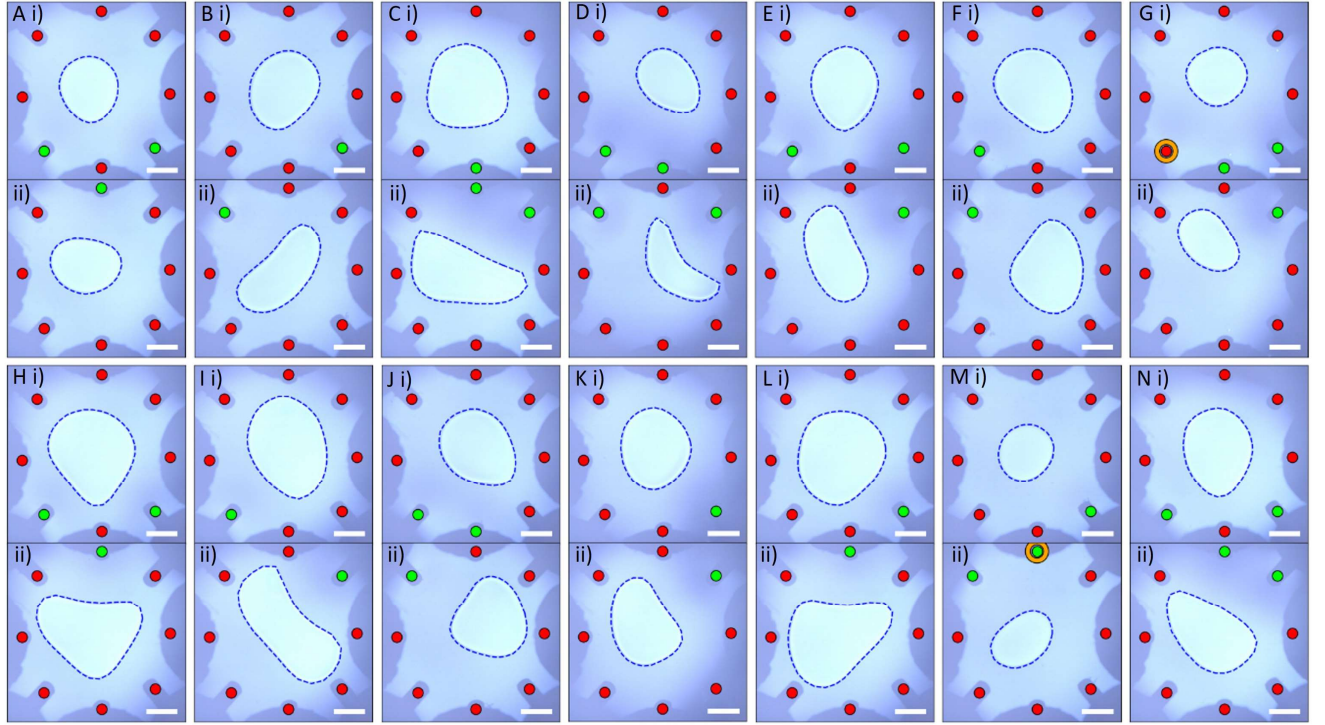


Figure 6. Inverse predictions of the actuation sequence for shapes of a hexadecane droplet at the air-ferrofluid interface for 14 sequences. The solenoids to be actuated are denoted by green indicators, and the ones to be inactivated are marked with red indicators. The orange encircles on the indicators represent the false predictions. The scale bars are 2 mm.

We measured the shape error as the mean absolute error between the predicted and actual shape radiuses for the first and second actuations as shown in Fig. 5a and 5b, respectively. The shaping errors are 0.16 ± 0.09 , 0.15 ± 0.10 , 0.13 ± 0.11 , 0.19 ± 0.09 , and 0.18 ± 0.11 mm for the first actuation and 0.47 ± 0.50 , 0.29 ± 0.27 , 0.36 ± 0.20 , 0.31 ± 0.20 , and 0.18 ± 0.19 for the second actuation of A, B, C, D, and E sequences, respectively. The prediction error for the second step is higher than the prediction error for the first step, which could be attributed to the accumulation of errors as the sequence progresses. However, the predicted and actual shapes are correlated with a maximum error of 1.70 mm for the second actuation observed in sequence A in the validation set. The variation between predicted and actual shapes is minimal for the first step of the sequence. The deviations between predicted and actual shapes could be attributed to the small size of the dataset, evaporation of the liquids, temperature changes, and chemical interactions at the interface of the hexadecane droplet and the ferrofluid. In our dataset, almost all the sequences involve convex shapes of the droplet for the first actuation. The second actuation may cause the droplet to turn into a concave shape.

The inverse prediction results for 14 sequences of the validation set are shown in Fig 6. The training accuracy was 73.9%. The accuracy of inverse predictions for the validation set is 79.1%. The false predictions in Sequence G and M are encircled in orange. The inverse model can correctly predict the required actuation sequence for a variety of droplet morphologies including convex and concave shapes.

IV. CONCLUSION

In this work, we reported a method to learn the evolution of the shape of a hexadecane droplet at an air-ferrofluid interface due to the sequential actuation of electromagnetic actuators. We can predict the shape of the droplet due to sequences of actuations using an LSTM-based model. The droplet shape can be either convex or concave. We can also predict the required sequence of actuation for a given shape sequence with an accuracy of 79.1% using an inverse model based on LSTM. Both models are able to capture the time-dependent behavior of the air-liquid-liquid system and the spreading phenomena of the hexadecane droplet at the air-liquid interface, and the predictions are promising. However, due to the tedious experimental procedure, the dataset used in this study is relatively small. To use the inverse model to predict the actuation sequence for arbitrary shapes, a larger dataset is needed to improve its prediction capability. The proposed method could be adapted to various systems which require the shaping of liquid droplets or soft matter in a sequential manner. Additionally, the learned model can serve as a simulation environment for training a reinforcement learning agent, enabling it to learn and improve its decision-making capabilities through interactions and feedback with the model. In this work, the magnetic flux density at the solenoid tip was constant during the sequence. In the case of variable magnetic flux density, the amount of data required can be larger compared to discrete values. Future work may include utilizing data-efficient exploration methods to predict the actuation required to generate the target shape which may be more suitable for situations where the action space is continuous, experiments are expensive and time-consuming.

REFERENCES

- [1] R. Song, S. Cho, S. Shin, H. Kim, and J. Lee, "From shaping to functionalization of micro-droplets and particles," *Nanoscale Adv.*, vol. 3, no. 12, pp. 3395–3416, 2021.
- [2] M. J. Hancock *et al.*, "Designer hydrophilic regions regulate droplet shape for controlled surface patterning and 3D microgel synthesis," *Small*, vol. 8, no. 3, pp. 393–403, 2012.
- [3] R. Raj, S. Adera, R. Enright, and E. N. Wang, "High-resolution liquid patterns via three-dimensional droplet shape control," *Nat. Commun.*, vol. 5, pp. 1–8, 2014.
- [4] X. Zhong, J. Ren, K. S. L. Chong, K. S. Ong, and F. Duan, "Controlling Octagon-to-Square Wetting Interface Transition of Evaporating Sessile Droplet through Surfactant on Microtextured Surface," *ACS Appl. Mater. Interfaces*, vol. 10, no. 14, pp. 11425–11429, 2018.
- [5] S. Nagelberg *et al.*, "Reconfigurable and responsive droplet-based compound micro-lenses," *Nat. Commun.*, vol. 8, 2017.
- [6] S. Ehrig *et al.*, "Surface tension determines tissue shape and growth kinetics," *Sci. Adv.*, vol. 5, no. 9, pp. 1–9, 2019.
- [7] Y. Bin Lee, O. Jeon, S. J. Lee, A. Ding, D. Wells, and E. Alsborg, "Induction of Four-Dimensional Spatiotemporal Geometric Transformations in High Cell Density Tissues via Shape-Changing Hydrogels," *Adv. Funct. Mater.*, vol. 31, no. 24, pp. 1–9, 2021.
- [8] Y. Tian and E. A. Lipke, "Microfluidic Production of Cell-Laden Microspheroidal Hydrogels with Different Geometric Shapes," *ACS Biomater. Sci. Eng.*, vol. 6, no. 11, pp. 6435–6444, 2020.
- [9] W. Bouwhuis, K. G. Winkels, I. R. Peters, P. Brunet, D. Van Der Meer, and J. H. Snoeijer, "Oscillating and star-shaped drops levitated by an airflow," *Phys. Rev. E - Stat. Nonlinear, Soft Matter Phys.*, vol. 88, no. 2, pp. 1–11, 2013.
- [10] E. H. Trinh, "Compact acoustic levitation device for studies in fluid dynamics and material science in the laboratory and microgravity," *Rev. Sci. Instrum.*, vol. 56, no. 11, pp. 2059–2065, 1985.
- [11] G. Raju, N. Kyriakopoulos, and J. V. I. Timonen, "Diversity of non-equilibrium patterns and emergence of activity in confined electrohydrodynamically driven liquids," *Sci. Adv.*, vol. 7, no. 38, pp. 1–9, 2021.
- [12] Y. Tokuda *et al.*, "Programmable liquid matter: 2D shape drawing of liquid metals by dynamic electric field," *Proc. 2017 ACM Int. Conf. Interact. Surfaces Spaces, ISS 2017*, pp. 454–457, 2017.
- [13] W. Yan, C. Zhao, W. Luo, W. Zhang, X. Li, and D. Liu, "Optically Guided Pyroelectric Manipulation of Water Droplet on a Superhydrophobic Surface," *ACS Appl. Mater. Interfaces*, vol. 13, no. 19, pp. 23181–23190, 2021.
- [14] N. Denkov, S. Tcholakova, I. Lesov, D. Cholakova, and S. K. Smoukov, "Self-shaping of oil droplets via the formation of intermediate rotator phases upon cooling," *Nature*, vol. 528, no. 7582, pp. 392–395, 2015.
- [15] X. Fan, X. Dong, A. C. Karacakol, H. Xie, and M. Sitti, "Reconfigurable multifunctional ferrofluid droplet robots," *Proc. Natl. Acad. Sci. U. S. A.*, vol. 117, no. 45, pp. 27916–27926, 2020.
- [16] R. Ahmed, M. Ilami, J. Bant, B. Beigzadeh, and H. Marvi, "A Shapeshifting Ferrofluidic Robot," *Soft Robot.*, vol. 00, no. 00, pp. 1–12, 2020.
- [17] T. Jamin, Y. Djama, J.-C. Bacri, and E. Falcon, "Tuning the resonant frequencies of a drop by a magnetic field," *Phys. Rev. Fluids*, vol. 1, no. 2, pp. 1–9, 2016.
- [18] X. Li *et al.*, "Programmable Digital Liquid Metal Droplets in Reconfigurable Magnetic Fields," *ACS Appl. Mater. Interfaces*, vol. 12, no. 33, pp. 37670–37679, 2020.
- [19] P. M. Vlahovska, "Electrohydrodynamics of drops and vesicles," *Annu. Rev. Fluid Mech.*, vol. 51, pp. 305–330, 2019.
- [20] K. Peddireddy, S. Čopar, K. V. Le, I. Mušević, C. Bahr, and V. S. R. Jampani, "Self-shaping liquid crystal droplets by balancing bulk elasticity and interfacial tension," *Proc. Natl. Acad. Sci. U. S. A.*, vol. 118, no. 14, pp. 1–7, 2021.
- [21] P. A. D. Harischandra, T. Välisalmi, Z. M. Cenev, M. B. Linder, and Q. Zhou, "Shaping Liquid Droplets on an Active Air – Ferrofluid Interface," vol. 39, 2023.
- [22] S. Hochreiter, "Long Short-Term Memory," vol. 1780, pp. 1735–1780, 1997.
- [23] F. A. Gers, J. Schmidhuber, and F. Cummins, "Learning to forget: Continual prediction with LSTM," *Neural Comput.*, vol. 12, no. 10, pp. 2451–2471, 2000.
- [24] W. Bai *et al.*, "Task-Based LSTM Kinematic Modeling for a Tendon-Driven Flexible Surgical Robot," *IEEE Trans. Med. Robot. Bionics*, vol. 4, no. 2, pp. 339–342, 2022.